Hsu *et al. Nanoscale Research Letters* (2022) 17:113
https://doi.org/10.1186/s11671-022-03754-9

Nanoscale Research Letters

RESEARCH

Open Access

Effects of ITO Contact Sizes on Performance of Blue Light MicroLEDs

Yu-Hsuan Hsu[1], Yu-Yun Lo[1], Yi-Hsin Lin[1], Hsiao-Wen Zan[1] and Ray-Hua Horng[2*]

Abstract

In this study, the effect of ITO contact ratio for blue light micro-light-emitting diode (μLED) with dimensions 40 μm × 40 μm was assessed. The contact ratio from 0.2 to 0.8 was designed for the ratio of electrode area to light-emitting area. As the contact ratio increased from 0.2 to 0.8, the turn-on voltage of μLED decreased. It could be due to the short lateral diffusion length in multiple quantum wells (MQW) and lower parallel resistance for the μLED with a large contact ratio. The leakage currents of single μLED were below 5.1×10^{-9} A, no matter the contact ratio. It means that the contact ratio does not affect the leakage current as measured on single chip. Moreover, μLED array with a 0.8 contact ratio presented the highest output power than other samples (5.25 mW as the current density of 1875 A/cm^2). It could attribute to the MQWs usage, the metal contact reflective behavior and less current crowding, which generated more carriers and extracted more lighting from the μLED. The simulation data using SpeCLED software agreed well with these experiments, and μLED with a 0.8 contact ratio showed the best optoelectronic properties.

Keywords: Micro-LED, Contact ratio, Blue light, Current crowding

Introduction

The leading display technologies are based on liquid–crystal display (LCD) and organic light-emitting diode (OLED), which almost dominate the display market. Even though LEDs as the backlight for LCD are very mature, due to high-efficiency, brightness, color purity, and self-emission [1, 2], micro-light-emitting diodes (μLEDs) have attracted much attention in high-resolution display applications. Compared with traditional LCDs, μLEDs exhibit higher energy efficiency, resolution, contrast, stability, and longer life. They can also be applied to very huge, transparent, or wearable displays of any shape [3, 4]. Moreover, developing smartphones, pads, wearable devices, and augmented/virtual reality (AR/VR) products lead to a growing commercial demand for high-performance μLEDs. However, a full-color μLEDs display on the same active materials, including red, blue, and green subpixels, is the primary requirement for simplified processing. Traditionally, InGaN epitaxy layers were used for blue and green color LEDs, and AlGaInP materials were applied to fabricate red color LEDs [5–7]. Integrating full-color subpixels is challenging due to the heterostructure and different substrates. To solve this problem, different colors of quantum dots (QDs) excited by a high-energy light source, such as UV and blue-light wavelengths, were developed in the past years [8–10].

Although LEDs have many advantages in optoelectronic performances, as the size of the chip shrinks to below 100 μm (called μLEDs), some issues were induced and affected the properties of devices significantly [11, 12]. For example, sidewall defects are created by an inductively coupled plasma reactive ion etching (ICP-RIE) [13–15]. These defects result in the Shockley–Read–Hall non-radiative recombination and further decreasing the efficiency of μLEDs. Previous studies were focused on the smooth morphology of the sidewall and passivation by a high-quality passivation layer using atomic layer deposit [16–18], which can repair the sidewall defect and avoid the non-radiative

*Correspondence: rayhua@nycu.edu.tw

[2] Institute of Electronics, National Yang Ming Chiao Tung University, Hsinchu 30010, Taiwan, ROC
Full list of author information is available at the end of the article

recombination behavior. Nevertheless, the electrode dimension effects on the performance of μLEDs were not studied, especially for the high-efficiency blue light μLEDs. To prevent deviations from the fabricated process of μLEDs, a chip size of 40 μm × 40 μm was used in this study. Meanwhile, the effect of the contact ratio can be observed more clearly in this chip size. The contact ratio of the ITO and electrode area to the emission area from 0.2 to 0.8 was studied. There were top-electrodes of μLEDs with 8 μm × 8 μm, 16 μm × 16 μm, 24 μm × 24 μm, and 32 μm × 32 μm, respectively, for the 0.2, 0.4, 0.6, and 0.8 contact ratios. The optoelectronic characteristics of μLEDs were measured and evaluated, including emission output power, wall-plug efficiency (WPE), and external quantum efficiency (EQE). We also discuss herein a simulation of the current distribution and characteristics for different contact ratio chips.

Experimental

The μLEDs were grown on sapphire substrate with 450 nm wavelength blue light emission. First, a buffer GaN was grown on c-plane sapphire, then grown a Si-doped n-GaN layer. The Mg-doped p-GaN layer and the active layer were contained by InGaN/GaN multiple quantum wells (MQWs). Therefore, an electron blocking layer was stacked between p-GaN and MQWs, which could control the current flow direction and prevent overflow leakage from the n-GaN layer to the p-GaN layer. A 300 nm ITO was grown on the p-GaN epilayer for the top Ohmic contact processing. Figure 1a showed the epilayer structure of blue light LEDs, and the schematic of μLED fabrication in this study was also presented shown in Fig. 1b. The standard LED development processes, such as photolithography, ICP-RIE dry etching, dielectric passivation layer deposited using plasma-enhanced chemical vapor deposition

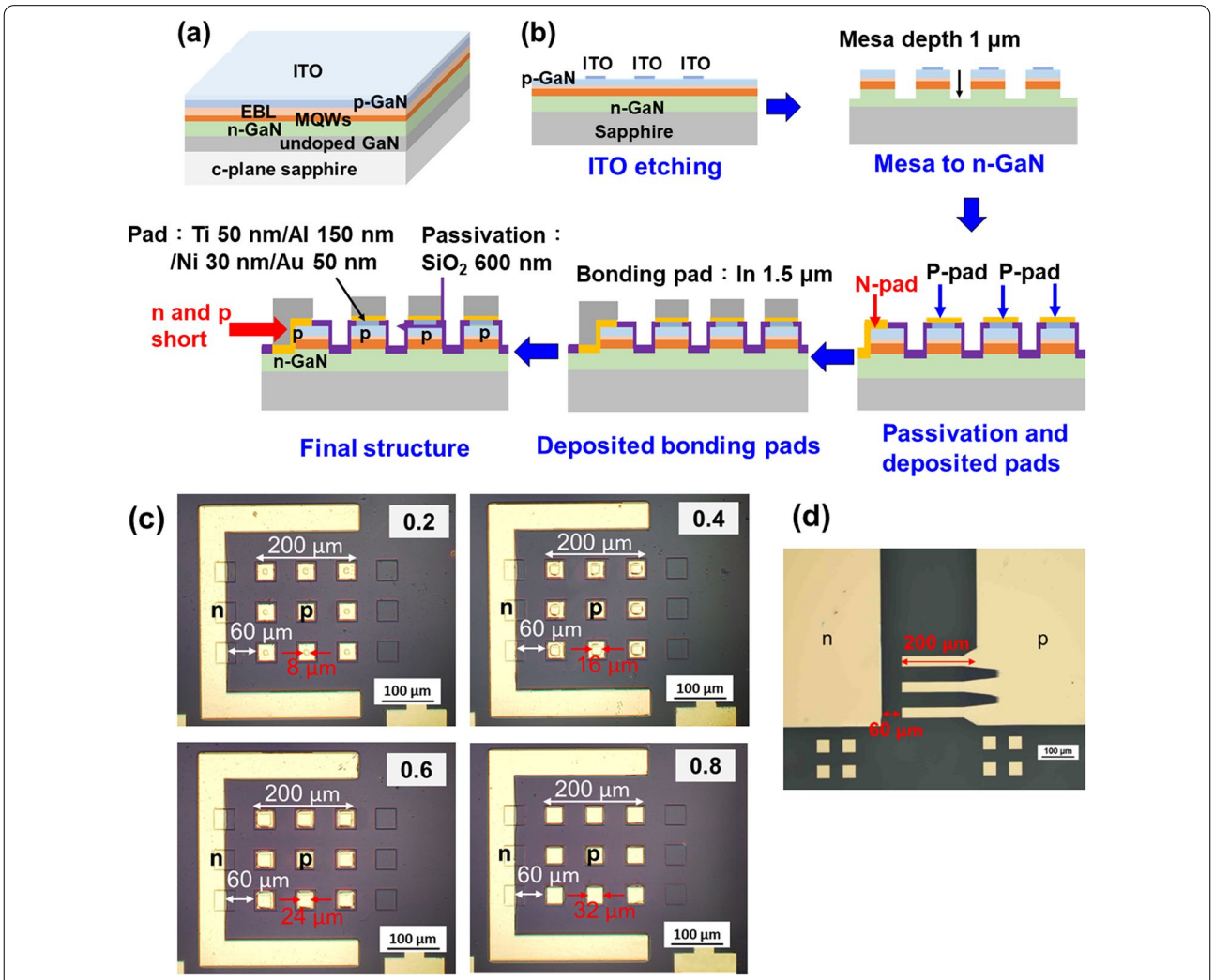

Fig. 1 **a** epi-layer structure, **b** μLED fabricated process flow, **c** 3 × 3 arrays, and **d** the circuit design in this study

(PECVD), metal evaporation, and lift-off for the contact pads, are shown in Fig. 1b. First, the indium tin oxide (ITO) layer was wet-etched using an ITO etching solution and defined the four-size contact sizes on the μLEDs with 40 μm × 40 μm dimension. The mesa structure was obtained by GaN etching with the gas of 20 sccm Cl_2 and 30 sccm BCl_3 in 5 mTorr to determine the active region 40 × 40 μm by ICP-RIE and the etching depth was 1 μm. After that, the 600 nm SiO_2 passivation layer was grown by PECVD, and the dry etching process opened for the metal contact area. Meanwhile, the n and p electrodes of the stack of Ti/Al/Ni/Au with 50 nm/150 nm/30 nm/50 nm were deposited on the passivation layer with open contact pads by an E-gun evaporation system, then deposited 1.5 μm thick indium with 32 μm × 32 μm by a thermal evaporator for the flip-chip process. Moreover, in order to let the bonding pads for n and p have the same height, the n ohmic contact pad was deposited on the sidewall and connected to p layer of one chip, shown in the red arrow in Fig. 1b. On the other hand, it is necessary to bond the μLED to the circuit board using the similar flip chip technology. If there is no sidewall protection using the passivation layer, the μLEDs should be easily short or present large leakage after bonding to circuit board.

To investigate the effect of different metal contact areas in μLED device, a laser direct writing system (MLA-150, Heidelberg Instruments) was applied for the photolithography process without the mask in this study, which technology can align accurately for smaller pattern design and also can reduce the cost to fabricate the mask. The size of μLED chips was 40 μm × 40 μm, and the ITO contact sizes were adjusted from 8 μm × 8 μm to 32 μm × 32 μm, as shown in Fig. 1c. The output power of single μLEDs was too low to measure. Therefore, the μLEDs array with three by three was designed. The metal layers of Ti/Al/Ni/Au (50/500/30/60 nm) deposited on the double-sides polished sapphire substrate were used as circuit electrodes for the μLEDs array package (Fig. 1d). Finally, the μLEDs array was flip chip bonded on the circuit under a bonding temperature of 220 °C and the pressure of 25 N for 5 min. After packaged, the light emission of the μLEDs array was from the backside of sapphire.

After processing, the electrical and optical properties of all μLEDs were measured at room temperature. Current–voltage (*I–V*) characteristics of the single chip μLED were investigated using a semiconductor parameter analyzer (2400 Source Meter; Keithley) by on-wafer measurement. Then, a charge-coupled device (CCD) was used to observe the corresponding emission pattern. After the In-Au bonding and TO-Can packaging, the output powers of the μLED array were measured with a calibrated integrating sphere.

Besides μLED manufacture, the results of the simulation by SpeCLED were also presented. Based on the power device parameters (power chip size in 1000 μm × 1000 μm at the operation current 350 mA), the total input current at 0.56 mA (current density 35 A/cm^2) was used for the μLEDs with 40 μm × 40 μm dimension. The properties of the ITO contact ratio of μLEDs with contact ratios from 0.2 to 0.8 were evaluated and discussed by current distribution, light output power, external quantum efficiency (EQE), and wall-plug efficiency (WPE).

Result and discussion

Figure 2A shows the forward I-V characteristics of the single chip μLED with the different contact ratio. The turn-on voltage of single chip μLED with the contact ratio from 0.2 to 0.8 was 2.79, 2.61, 2.57, and 2.54 V, respectively. The corresponding dynamic resistance was 16.67, 4.62, 2.17 and 1.3 kΩ at the voltage of 3 V. When the ITO contact ratio increased from 0.2 to 0.8, the forward voltage of μLEDs array decreased from 3.58 to 2.83 V at 1 mA injection current. The μLEDs with contact ratios of 0.6 and 0.8 presented lower turn-on voltage and dynamic resistance. It could be attributed to the larger ITO contact pad area resulting in the lower current density at the same current injection. As the μLED was turned on, there existed many parallel resistances (R1), as shown in the inset of Fig. 2a. It can contribute to low equivalent resistance, which can be fitted and calculated in Fig. 2b. The parallel resistances R1, which can be calculated as the I-V operated at the low voltage range shown in Fig. 2b, were obtained at 1.16, 0.94, 0.93, and 0.63Ω when the contact ratio varied from 0.2 to 0.8. For a 0.2 contact ratio, the ITO contact pad of the μLED was only 8 μm × 8 μm, and for a 0.8 contact ratio, the dimension of the ITO contact pad of the μLED was 32 μm × 32 μm. Besides the parallel resistances under the pad, there is an additional equivalent series resistance R2, as shown in the inset of Fig. 2a. This series resistance decides how current laterally spread out of the contact area and flows into QW. It can be calculated as the I–V operated at the high voltage range shown in Fig. 2b. Hence, the total resistance was not directly inversely proportional to the contact pad area. Because of lower equivalent resistance, a lower forward voltage was observed for the μLED with contact ratios of 0.6 and 0.8 samples under the same injection current. A large contact pad area can contribute to the uniform current distribution, resulting in low resistance. As the contact ratio increased from 0.2 to 0.8, the value of series resistances R2 could decrease and was calculated at 250.6, 173.4, 120.4, and 117.4Ω, respectively.

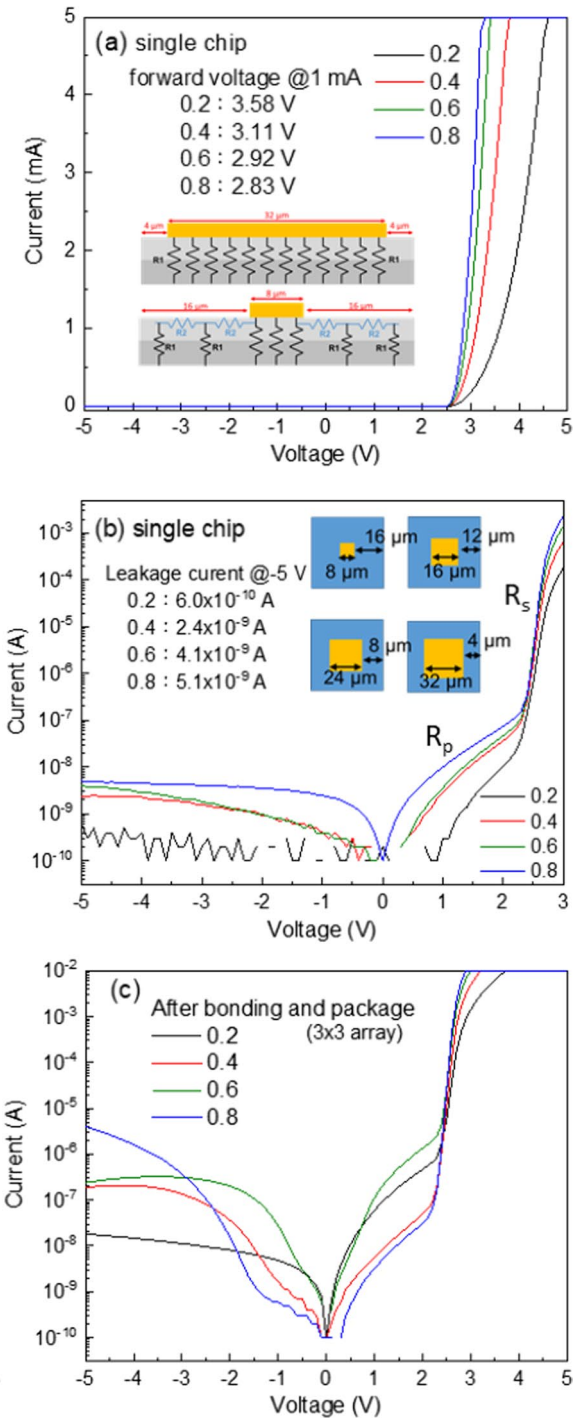

Fig. 2 I-V characteristic **a** in linear-scale **b** log scale on-chip measurement, and **c** I–V characteristic in log scale after flip-chip and wire bonding from − 5 to 5 V of different contact ratios

The main issue in μLED with a large contact pad is the leakage current, which affects device properties significantly. Figure 2b shows the reverse current as a function of reverse voltage for all μLEDs. As the contact ratio increased, the leakage currents were slightly raised from 6×10^{-10} A to 5.1×10^{-9} A measured from single chip before bonding. The leakage current of μLEDs with different contact ratios was all less than 5.1×10^{-9} A at the reversed voltage of − 5 V. Although the distance from the edge of the ITO contact pad to the sidewall was only 4 μm for μLED with a contact ratio of 0.8, as shown in the inset of Fig. 2b, the leakage current was still very low. This indicated that in this chip size, the leakage current did not increase as the contact ratio increased, and a weak relationship was observed between the leakage behavior and the contact pad area. The first reason would be that the SiO_2 passivation layer deposited by PECVD can effectively protect the sidewall area from leakage for μLED with a 0.8 contact ratio with 4 μm distance from the edge of ITO to side wall. The other reason would be the relatively more considerable sheet resistance in the p-GaN layer (due to the low mobility hole), which limits the spread of the current. The lower lateral carrier diffusion length (< 5 μm) in the InGaN quantum well was due to the random alloy fluctuation [19, 20]. Nevertheless, the SiO_2 passivation could be contribute to the low leakage current because the metal contact pad and ITO to the sidewall was only 4 μm for μLED with a contact ratio of 0.8 which is within the hole diffusion length. The above I-V characteristics exhibited that the contact ratio affects the resistance, which further affects the forward voltage in each μLED. Therefore, the ideality factor of 0.2, 0.4, 0.6, and 0.8 contact ratios were calculated using the slopes of the I-V curve in the log scale and also listed in Table 1. The ideality factor exhibited the highest value in 0.2 contact ratio in 2.43. As the contact ratio increased from 0.4, 0.6 to 0.8, the corresponding ideality factor of μLED decreased in 2.19, 2.02, and 1.95. It was well known that the recombination carrier of the current domain is in a small forward voltage, the ideality factor is generally 2.0. Exceeding 2.0 is due to the defect-assisted tunneling domain of the conducting mechanism [19, 21]. In this result, the contact ratio of 0.6 and 0.8 present better electrical properties. As concerning the μLEDs with 0.2 and 0.4 contact ratio, due to higher resistance and low current spreading, defect-assisted tunneling could be easily occurred in these two samples.

Furthermore, the leakage current of μLEDs was also measured after the flip-chip. The current in the log scale as a function of voltage is presented in Fig. 2c. The leakage current of the nine μLEDs at -5 V increased from 1.8210^{-8} to 3.9510^{-6} A as contact ratio increased from 0.2 to 0.8. Obviously, after flip chip packaged, the larger contact resulted in the leakage current increasing even the chips has been passivated by SiO_2. Therefore, it is important to evaluate whether the contact ratio affects the optoelectronics in the μLEDs with 3×3 arrays.

Table 1 Contact size and electric-optical properties in this study

40 × 40 μm	Contact size	Ideality factor	Output power$_{max}$	WPE$_{max}$ (%)	EQE$_{max}$ (%)
0.2	8 × 8 μm	2.43	2.27 mW	9.61	9.43
0.4	16 × 16 μm	2.19	3.51 mW	10.46	10.16
0.6	24 × 24 μm	2.02	4.63 mW	11.08	10.76
0.8	32 × 32 μm	1.95	5.25 mW	11.24	10.84

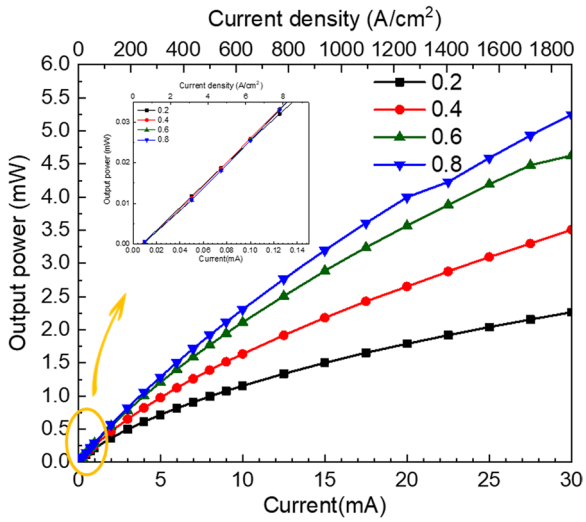

Fig. 3 The emission output power of different contact ratios

Figure 3 shows the optical output power of the nine μLEDs array as a function of the injection current and injection current density (top x-axial). With the increase in the injection current, the output power increased for all μLEDs array with different contact ratios, and the μLEDs array with 0.8 contact ratio had a larger slope than the other μLEDs. When the injection current increased from 0.01 to 30 mA, the output powers of μLEDs array with 0.2, 0.4, 0.6, and 0.8 contact ratios were raised from 0.0006 to 2.27 mW, 0.004 to 3.51 mW, 0.004 to 4.63 mW, and 0.004 to 5.25 mW, respectively. The inset of Fig. 3 showed the emission output power in a small injection current. The output power of the 0.2 contact ratio was slightly higher than other contact ratios when the injection currents were 0.05 and 0.075 mA. The 0.2 contact ratio has a higher local current density at the same total current; therefore, it reached the internal quantum efficiency (IQE) peak earlier than other cases, leading to the highest output power. However, the droop effect also happens earlier as the current density increases, which lead to a smaller output power curve slope. The highest output power of μLEDs array was in contact ratio 0.8 as injection current from 0.1 to 30 mA. If the contact ratio is too small, the current crowding affected the performance obviously, which also has a poor spread of the current in a small contact ratio. The electrical characteristic of the μLEDs array also affected the emission output power. Moreover, the μLEDs with a larger contact ratio can contribute to more light reflecting toward the sapphire side and enhance the output power [22]. In this work, the performance of μLEDs were evaluated by injection current from 0.01 to 30 mA. Because the injected current was used to drive 9 chips, it means 1 μA to 3.33 mA for one chip with 40 μm 40 μm. This discussion current is a good range which cover high IQE at low current density for VR application and high power output at high current density for AR application.

The EQE as the function of injection current and injection current density was plotted and is shown in Fig. 4a. In the small injection current region as shown in the inset of Fig. 4a, the μLED array with small contact ratio 0.2 presented the highest EQE than those of μLEDs with other contact ratios as injection small current at 0.05 and 0.1 mA. However, as the injection current increased from 0.05 to 30 mA, the EQE curve of μLED array with a 0.2 contact ratio dropped significantly as compared to those of μLED array with the wide contact ratios in Fig. 4. This phenomenon was also observed in the emission output power shown in Fig. 3. The μLED with 0.2 contact ratio has outstanding performance than other μLEDs in small injection current because the higher current density was obtained for the μLEDs with a 0.2 contact ratio. Nevertheless, as the injection current increased, the current crowding occurred and the current spreading limited the usage of MQWs, which caused the EQE to decrease intensely from 9.43 to 2.72% of μLED with 0.2 contact ratio. In contrast, the EQE of μLEDs array with 0.8 contact ratio decreasing was alleviated from 10.84 to 6.35% as the injection current increased to 30 mA. The highest EQE value was observed at injection currents 0.15, 0.25, 0.5, and 0.75 mA as the contact ratio increased from 0.2 to 0.8, and the EQE were 9.43, 10.16, 10.76, and 10.84%, respectively.

The other important property is the WPE of these devices. The WPE as a function of current injection for the μLED with different contact ratios is presented in Fig. 4b. As the injection current increased, the WPE of μLEDs array with contact ratios 0.2, 0.4, 0.6, and 0.8

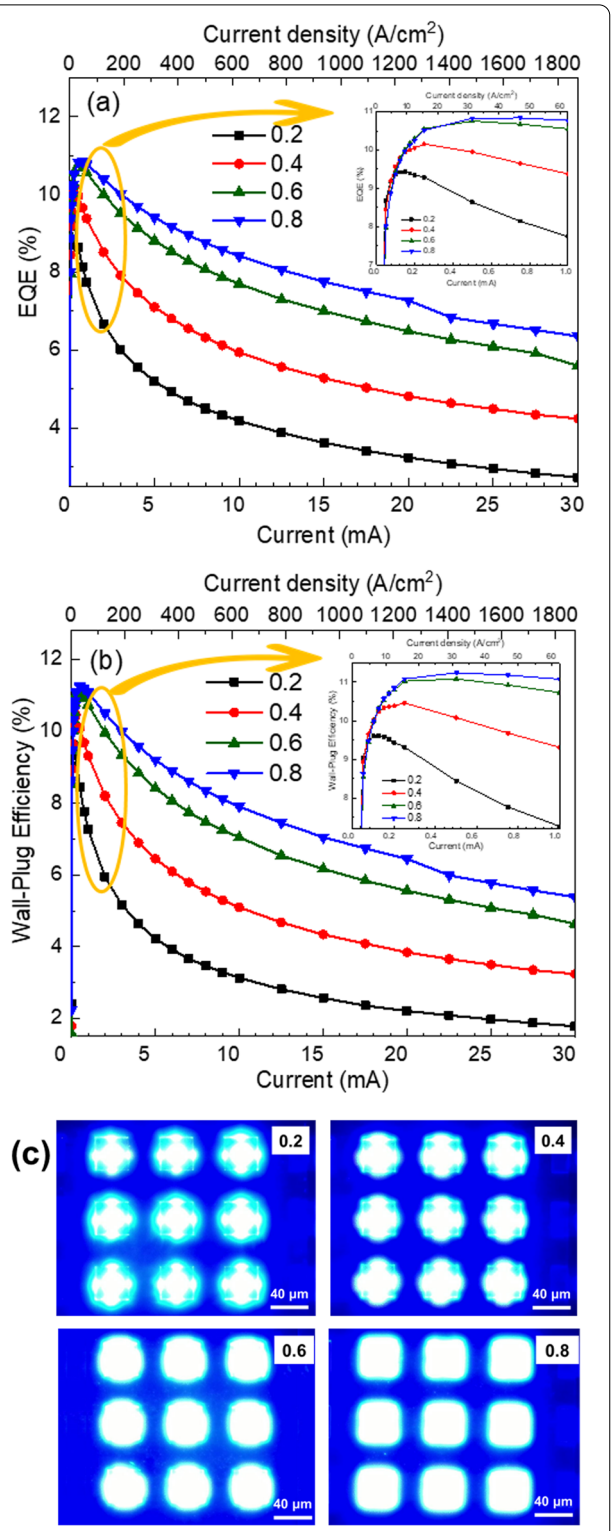

Fig. 4 **a** EQE, **b** wall-plug efficiency of different contact ratios, and **c** emission pictures at 1 mA (62.5 A/cm^2) for different contact ratio

decreased from 9.61 to 1.79%, 10.46 to 3.24%, 11.08 to 4.63%, and 11.24 to 5.38%, respectively. The inset of Fig. 4b shows the WPE of μLEDs array at a small current injected from 0.05 to 1 mA. The obtained results were very similar to those of EQE results discussed above. In the μLEDs array with 0.2 contact ratio, the WPE of μLEDs array was slightly higher than other contact ratios at 0.05 mA injection current, then decreased dramatically when the injection current increased from 0.1 to 30 mA; it could be because of a higher forward voltage in the 0.2 contact ratio. Since the WPE is output light power/IV, the applied voltage was much larger in the case of a 0.2 contact ratio. The μLEDs with a 0.8 contact ratio presented the highest WPE at 11.24%. The above conclusion can be also demonstrated by the emission patterns for the μLEDs with different contact ratios as 1 mA injection current, as shown in Fig. 4c. The emission area presented the largest and most uniform for the μLEDs with a 0.8 contact ratio. At a contact ratio below 0.4, the light is only emitted around the contact area. Due to the less usage of the MQW area, the carrier reconvened only in the injection region. Meanwhile, the emission uniformity at the uLEDs with 0.2 and 0.4 contact ratios were both very disappointing and emitting an asymmetric pattern. In contrast, the uLED with 0.6 and 0.8 contact ratios presented more symmetry and uniformity. Furthermore, the uLEDs with 0.8 contact ratio presented a square shape which was matched to the injection area than that of uLED with 0.6 contact ratio.

Finally, to understand the lateral carrier distribution, the SpeCLED software was used to simulate the current density distribution for μLED with different ITO contact ratios. Figure 5 presents the simulation results of current density distribution in the lateral direction for μLEDs with different contact ratios. A constant injection current, 0.56 mA, was used to drive the μLEDs for the simulation. The obtained characteristics of the device calculated by simulation software, including the forward voltage, output power, wall-plug efficiency, and EQE, are listed in Table 2. This table shows that as the contact ratio increased from 0.2 to 0.8, forward voltage decreased from 2.80 to 2.59 V. This simulation result was consistent with the measurement data from the experiment performed in this study. As mentioned above, the parallel resistance decreased as the contact ratio increased, which led to a decrease in the forward voltage. Moreover, emission output power, wall-plug efficiency, and EQE were all enhanced as the contact ratio increased. The uLEDs with contact ratio 0.8 exhibited the highest output power, wall-plug efficiency, and EQE peak. The values were 0.204 mW, 14.04%, and 11.73%, respectively. The obtained simulation results agreed well with the experiment results.

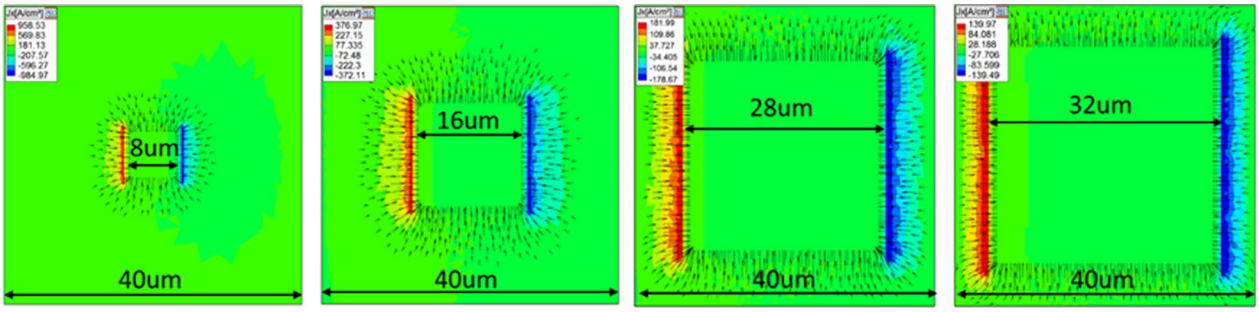

Fig. 5 Current spreading simulation results for different contact ratios

Table 2 Simulation data of different contact ratios in 40 μm × 40 μm chip size

40 μm × 40 μm	0.2	0.4	0.6	0.8
Forward bias [V]	2.80	2.65	2.61	2.59
Current [mA]	0.56			
Output power [mW]	0.125	0.164	0.187	0.204
Wall-plug efficiency [%]	7.98	11.12	13.02	14.04
EQE [%]	7.21	9.52	10.97	11.73

Conclusion

IN this study, the 3×3 blue light μLEDs arrays were fabricated for four ITO contact ratios in 40×40 μm^2 with contact sizes 8×8, 16×16, 24×24, and 32×32 μm^2 using a laser direct writing system without a mask. The turn-on voltage decreased from 2.8 to 2.5 V as the contact ratio increased due to the lower parallel resistance in widely contact ratio. Moreover, the leakage currents were below 5.1×10^{-9} A at the reverse bias − 5 V. The obtained results suggest that the passivation layer plays an excellent role in repairing the sidewall defect in these chip sizes and also indicate that the contact size did not induce leakage current in the bottom emitting μLEDs. Particularly, the contact ratio of 0.2 presented a higher emission output power and EQE in the small injection current region. This is attributed to the higher current density in the small injection current than the wide contact ratios. However, it further increased the injection current, the current crowding, and the current spreading will domain the optoelectronic performances in μLEDs. The optoelectronic characteristics exhibited an outstanding performance of the μLEDs contact ratio was 0.8. When injected with 0.5 mA current (current density 31.3 A/cm^2), the 0.8 contact ratio had the highest wall-plug efficiency and EQE; the values were 11.24% and 10.84%, respectively. Among this contact ratio, 0.8 also presented the strongest output power, 5.25 mW, as the injection current was 30 mA (current density 1875 A/cm^2).

The same result was obtained from the simulation; when the contact ratio increased, the turn-on voltage decreased from 2.8 to 2.6 V. The contact ratio of 0.8 had more outstanding properties than others. When the contact ratio increased from 0.2 to 0.6, the value of output power, wall-plug efficiency, and EQE increased significantly. Meanwhile, according to the current distribution, the MQWs usage efficiency was observed distinctly. It resulted that the 0.8 contact ratio showed an outstanding performance in this study.

Abbreviations

μLEDs: Micro-light-emitting diodes; ICP: Inductively coupled plasma; PECVD: Plasma-enhanced chemical vapor deposition; WPE: Wall-plug efficiency; EQE: External quantum efficiency; LCD: Liquid–crystal display; OLED: Organic light-emitting diode; AR/VR: Augmented/virtual reality; QDs: Quantum dots; ALD: Atomic layer deposit; MQWs: Multiple quantum wells; EBL: Electron blocking layer.

Acknowledgments

This study was also supported by Science Park Emerging Technology Application Program, Taiwan, R.O.C., under the grants 111AO29B. We acknowledge MA Tek for funding and material measurement support (Grant Number: 2022-T-018). We thank the National Nano Device Laboratory and Taiwan Instrument Research Institute for allowing us to use their facilities.

Author Contributions

YHH processed, simulated the LEDs structure and wrote the draft of this paper, YYL measured the LEDs characteristic, YHL analyzed the simulation results, HWZ analyzed the LED properties, and RHH provided the concepts, design the process and write the paper. All authors read and approved the final manuscript.

Funding

This study was supported by the National Science and Technology Council (NSTC), Taiwan, R.O.C., under the grants NSTC 109-2634-F-009-028, 110-2224-E-A49-003, and 110-2218-E-A49-020-MBK.

Availability of Data and Material

The datasets used and/or analyzed during the current study are available from the corresponding author on reasonable request.

Declarations

Ethics Approval and Consent to Participate

Not applicable.

Consent for Publication
All authors consent to the publication of this manuscript.

Competing Interests
The authors declare that they have no competing interests.

Author details
[1]Department of Photonics, College of Electrical and Computer Engineering, National Yang Ming Chiao Tung University, Hsinchu 30010, Taiwan, ROC. [2]Institute of Electronics, National Yang Ming Chiao Tung University, Hsinchu 30010, Taiwan, ROC.

Received: 14 October 2022 Accepted: 20 November 2022
Published online: 28 November 2022

References

1. Hang S, Chuang CM, Zhang YH, Chu CS, Tian KK, Zheng Q, Wu TZ, Liu ZJ, Zhang ZH, Li Q, Kuo HC (2021) A review on the low external quantum efficiency and the remedies for GaN-based micro-LEDs. J Phys D-Appl Phys 54(15):153002
2. Wang Z, Shan XY, Cui XG, Tian PF (2020) Characteristics and techniques of GaNbased micro-LEDs for application in next-generation display. J Semicond 41(4):041606
3. Anwar AR, Sajjad MT, Johar MA, Hernández-Gutiérrez CA, Usman M, Łepkowski SP (2022) Recent progress in micro-LED-based display technologies. Laser Photonics Rev 16(6):2100427
4. Hsiang EL, Yang ZY, Yang Q, Lan YF, Wu ST (2021) Prospects and challenges of mini-LED, OLED, and micro-LED displays. J Soc Inf Disp 29(6):446–465
5. Smith JM, Ley R, Wong MS, Baek YH, Kang JH, Kim CH, Gordon MJ, Nakamura S, Speck JS, DenBaars SP (2020) Comparison of size-dependent characteristics of blue and green InGaN microLEDs down to 1 μm in diameter. Appl Phys Lett 116:071102
6. Zhang SN, Zhang JL, Gao JD, Wang XL, Zheng CD, Zhang M, Wu XM, Xu LQ, Ding J, Quan ZJ, Jiang FY (2020) Efficient emission of InGaN-based light-emitting diodes: toward orange and red. Photonics Res 8(11):1671–1675
7. Horng RH, Chien HY, Chen KY, Tseng WY, Tsai YT, Tarntair FG (2018) Development and fabrication of AlGaInP-based flip-chip micro-LEDs. IEEE J Electron Devices Soc 6(1):475–479
8. Yan CM, Du XW, Li JS, Ding XR, Li ZT, Tang Y (2019) Effect of excitation wavelength on optical performances of quantum-dot-converted light-emitting diode. Nanomaterials 9(8):1100
9. Kim HM, Ryu M, Cha JHJ, Kim HS, Jeong T, Jang J (2019) Ten micrometer pixel, quantum dots color conversion layer for high resolution and full color active matrix micro-LED display. J Soc Inf Disp 27(6):347–353
10. Han HV, Lin H, Lin CC, Chong WC, Li JR, Chen KJ, Yu PC, Chen TM, Chen HM, Lau KM, Kuo HC (2015) Resonant-enhanced full-color emission of quantum-dot-based micro LED display technology. Opt Express 23(25):32504–32515
11. Chen Z, Yan SK, Danesh C (2021) MicroLED technologies and applications: characteristics, fabrication, progress, and challenges. J Phys D: Appl Phys 54(12):123001
12. Olivier F, Tirano S, Dupre L, Aventurier B, Largeron C, Templier F (2017) Influence of size-reduction on the performances of GaN-based micro-LEDs for display application. J Lumines 191:112–116
13. Boussadi Y, Rochat N, Barnes JP, Ben B, Ferrandis P, Masenelli B, Licitra C (2021) Investigation of sidewall damage induced by reactive ion etching on AlGaInP MESA for micro-LED application". J Lumines 234:117937
14. Olivier F, Daami A, Licitra C, Templier F (2017) Shockley-Read-Hall and Auger non-radiative recombination in GaN-based LEDs: A size effect study. Appl Phys Lett 111(2):022104
15. Kou J, Shen CC, Shao H, Che J, Hou X, Chu C, Tian K, Zhang Y, Zhang ZH, Kuo HC (2019) Impact of the surface recombination on InGaN/GaN-based blue micro-light emitting diodes. Opt Express 27(12):A643–A653
16. Yeh YW, Lin SH, Hsu TC, Lai SQ, Lee PT, Lien SY, Wuu DS, Li GS, Chen Z, Wu TZ, Kuo HC (2021) Advanced atomic layer deposition technologies for micro-LEDs and VCSELs. Nanoscale Res Lett 16(1):164
17. Lee DH, Lee JH, Park JS, Seong TY, Amano H (2020) The electrochemical society, find out more improving the leakage characteristics and efficiency of GaN-based micro-light-emitting diode with optimized passivation. ECS J Solid State Sci Technol 9(5):055001
18. Wong MS, Hwang D, Alhassan AI, Lee C, Ley R, Nakamura S, DenBaars SP (2018) High efficiency of III-nitride micro-light-emitting diodes by sidewall passivation using atomic layer deposition. Opt Express 26(16):21324–21331
19. Shen HT, Weisbuch C, Speck JS, Wu YR (2021) Three-dimensional modeling of minority-carrier lateral diffusion length including random alloy fluctuations in (In, Ga)N and (Al, Ga)N single quantum wells. Phys Rev Appl 16(2):024054
20. Ho CH, Speck JS, Weisbuch C, Wu YR (2022) Efficiency and forward voltage of blue and green lateral LEDs with V-shaped defects and random alloy fluctuation in quantum wells. Phys Rev Appl 17(1):014033
21. Lee M, Lee H, Song KM, Kim J (2018) Investigation of forward tunneling characteristics of InGaN/GaN blue light-emitting diodes on freestanding GaN detached from a Si substrate. Nanomaterials 8(7):543
22. Liou JK, Liu YJ, Chen CC, Chou PC, Hsu WC, Liu WC (2012) On a GaN-based light-emitting diode with an aluminum metal mirror deposited on naturally-textured V-shaped pits grown on the p-GaN surface. IEEE Electron Device Lett 33(2):227–229

Publisher's Note